Spin-noise spectrum of hot vapor atoms in an anti-relaxation-coated cell

Yuanjiang Tang [2], Ya Wen [1,2], Ling Cai,[2] and Kaifeng Zhao [1,2,*]

[1]*Key Laboratory of Nuclear Physics and Ion-Beam Application (MOE), Fudan University, Shanghai 200433, China*

[2]*Institute of Modern Physics, Department of Nuclear Science and Technology, Fudan University, China*

(Received 15 September 2019; published 21 January 2020)

We study the spin-noise spectrum (SNS) of unpolarized Rb vapor in an evacuated anti-relaxation-coated cell using parametric Faraday rotation of a flat-top probe beam with variable diameter. We identify a distinct structure in the spectrum, called the Ramsey peak. We find that the power of the Ramsey peak is inversely proportional to the total number of atoms in the cell, and the power of the total spin noise is inversely proportional to the number of atoms within the probe beam. We further present a full theoretical analysis of the SNS by comparing three models of spin diffusion: Fickian diffusion, the ballistic flight, and Langevin's diffusion. We find that Fickian diffusion fails, while the ballistic flight is acceptable. However, Langevin's diffusion yields a remarkable agreement with the experimental spectrum.

DOI: 10.1103/PhysRevA.101.013821

I. INTRODUCTION

Spin-polarized atoms are the workhorse in many areas of precision measurements, such as the magnetometer [1–3], the gyroscope [4,5], tests of fundamental symmetry [6,7], and search of new physics [8,9]. Under ideal technical conditions, the measurement sensitivity is limited by the spin projection noise (SPN) of the atom and the photon shot noise (PSN) of the probe light. As one can increase the ratio of signal to PSN by increasing the spin polarization and the optical depth, SPN ultimately becomes the fundamental limit. For atomic magnetometry, suppose an atomic ensemble of spin J is fully polarized along the x direction, the $\mathbf{B}$ field to be measured is in the y direction, and the z component of spin polarization is used to estimate the field. If the total measurement time t_{M} is much longer than the spin's transverse relaxation time T_2, then the SPN limited sensitivity is given by [3,10]

$$\delta B_y = \frac{1}{\partial J_z/\partial B_y}\delta J_z \frac{1}{\sqrt{t_{\mathrm{M}}/T_2}} = \frac{1}{\gamma T_2 J}\sqrt{\frac{J}{2N}}\frac{1}{\sqrt{t_{\mathrm{M}}/T_2}}, \qquad (1)$$

where γ is the gyromagnetic ratio of the spin, N is the total number of measured spins.

One of the most important spin relaxation mechanisms in atomic vapor cells is the wall relaxation due to atoms colliding with the inner surface of the cell. One way to suppress the wall relaxation is to fill the cell with high-pressure inert buffer gases to slow down the diffusion of atoms towards the cell wall. Another way is to coat the cell wall with some anti-relaxation material such as paraffin, alkene, or octadecyltrichlorosilane (OTS), which can preserve the atomic spin coherence over hundreds to millions of wall collisions [11–15]. Anti-relaxation-coated cells (ACCs) play an important role in magnetometry [15–18], frequency standard [19,20], and testing new ideas of quantum information and quantum metrology [17,21,22]. Compared to buffer-gas-filled cells, the ACC has several advantages. The signals are much larger without the pressure broadening of optical resonances caused by buffer gases. Atoms diffuse in the cell so fast that all of them can be pumped without the need to expand the pump beam to cover the entire cell. Fast atomic diffusions also reduce by motional narrowing, the broadening of magnetic resonance in the case of inhomogeneous field or light shift. Finally, it seems to be accepted without experimental evidence that the fundamental sensitivity of magnetometry in the ACC is independent of the probe beam area [15,23]. The argument is that because atoms can collide many times with the cell wall and spread over the entire cell without losing their spin coherences, all of them are detected by the probe within the relaxation time T_2; hence the N in Eq. (1) represents the total number of atoms in the cell. Whereas in buffer-gas-filled cells, it was experimentally demonstrated that the power of spin noise is inversely proportional to the area of the probe beam [24].

Spin noise spectrum (SNS) provides rich information about the physical properties of unperturbed spin systems [25–27] from vapor atoms [24,28–30] to semiconductors [31–33]. The effects of spin diffusion on SNS was first studied for quantum wells [34]. Theories of the two-beam method have also been proposed for studying spin transport, diffusion, and spatial correlations [35,36]. SNS of vapor atoms in buffer-gas-filled cells has been thoroughly studied recently, yielding the analytical expression of the spin diffusion time-correlation function and the spectrum line shape [37,38]. However, there is no corresponding study on the SNS of atoms in ACCs, where not only the behavior of spin diffusion could be very different, but also boundary effects have to be included.

Here, we report a quantitative study on the SNS of an unpolarized atomic vapor in an OTS-coated cell using a flat-top probe beam with variable diameter. We first show that the total power of the SNS is inversely proportional to the beam area, whereas the power, as well as the shape of a substructure of the SNS, called the Ramsey peak, is independent of the beam area. The ratio between the two powers is equal to

*zhaokf@fudan.edu.cn

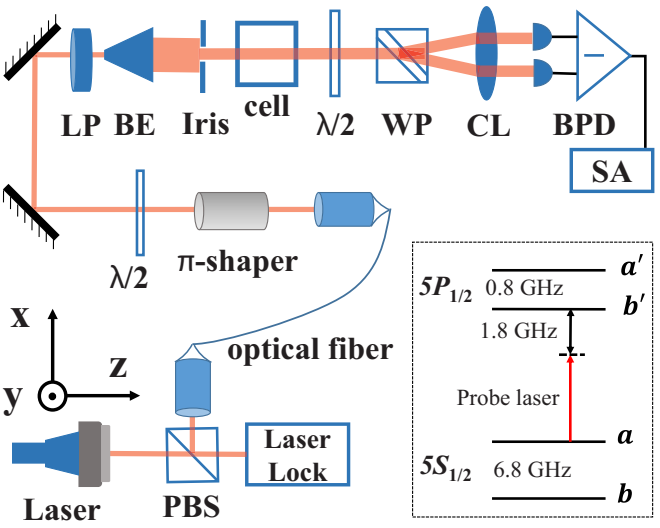

FIG. 1. Experimental setup. PBS, polarizing beam splitter; Laser lock, laser frequency locking module; $\lambda/2$, half-wave plate; π shaper, optical system converting a Gaussian beam into a flat-top beam; LP, linear polarizer; BE, beam expander; Iris, diaphragm for adjusting beam area; WP, Wollaston prism; CL, converging lens; BPD, balanced photon detector; SA, spectrum analyzer. Inset: probe frequency and the energy diagram of the ^{87}Rb $D1$ transition.

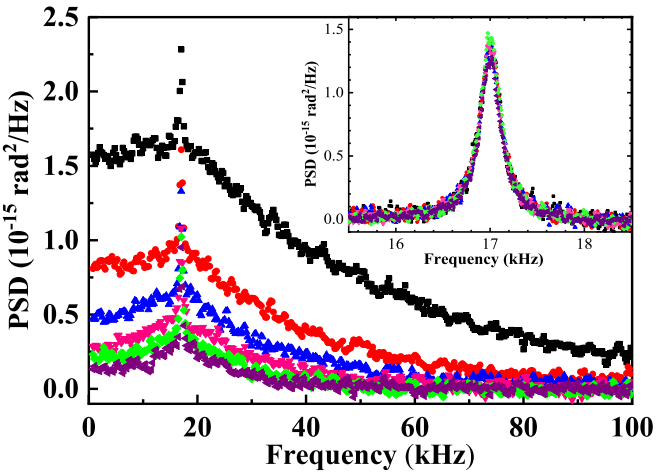

FIG. 2. Probe beam area dependence of the spin-noise spectrum taken at 0.024 G. The cell's tip and body temperatures are 104.4 °C and 107.1 °C, respectively. All data are taken with a constant probe power of 60 μW. (a) The SNS for different probe beam diameters. The main plot shows the SNS from a full frequency scan (100 kHz) of the SA. The resonance amplitude decreases with increasing probe beam diameter from 2 (black), 3 (red), 4 (blue), 5 (pink), and 6 (green) to 7 (purple) mm. The inset shows the SNSs of a 3.125-kHz frequency scan around the Ramsey peak with their transit bases subtracted.

the ratio between the cross-sectional area of the cell and the beam. Then, we give a full analysis of the SNS in the ACC by comparing three different models of bounded spin diffusion, including Fickian diffusion, ballistic flight, and Langevin's diffusion. All three models reproduce the same power relation. However, bounded Langevin's diffusion gives the best agreement of line shape between the theory and the experiment.

II. EXPERIMENTAL PROCEDURES

Our experimental setup is shown in Fig. 1.

A cubic Pyrex cell of 22 mm inner length containing isotopically enriched ^{87}Rb without buffer gas is placed in a ceramic oven, which is heated by a nonmagnetic wire with an ac of 71 kHz. The oven is designed to keep the cell's tip, which contains the Rb reservoir, a few degrees cooler than the body. The inner wall of the cell is coated with OTS [39] capable of preserving Rb spin coherences over several hundred wall collisions. A 30-cm-diameter Helmholtz coil controlled by a low-noise current source (ADC6156) provides a constant **B** field in the y direction. The whole system resides in a four-layer μ-metal shield with a residue field of several nT. The probe beam comes from a Toptica diode laser with its frequency locked about 1.8 GHz below the $F = 2$ to $F' = 1$ transition of the ^{87}Rb $D1$ line by a dichroic atomic vapor laser lock (DAVLL) system [40]. The probe is converted to a flat-top beam of 18 mm diameter by a single-mode optical fiber, a π shaper, and a beam expander. A variable diaphragm adjusts the beam's diameter d. A Wollaston prism, together with a balanced photon detector, measures the Faraday rotation (FR) θ of the probe at the exit of the cell. The FR signal is fed into a spectrum analyzer (SRS760) for power spectrum density (PSD) measurement. All spectra are averaged 5000 times. The SNS is obtained by subtracting the background PSD measured at $B = 0.45$ G from the PSD measured at $B = 0.024$ G.

We keep a constant light power for beams of different diameters so that the spin relaxation rate due to probe photon absorption stays the same. Such concern is unnecessary for large frequency detuning since the absorption relaxation is negligible compared to other relaxation processes. Thus, the same experimental results can be obtained by using probe beams of different diameters with constant intensity.

The main plot of Fig. 2 shows that the SNS consists of a broad base and a narrow tip at the Larmor frequency of the **B** field. Since the probe does not cover the vapor cell, the precession signal of a spin fluctuation is interrupted by atoms flying out of the beam, creating the transit broadening base in the SNS. However, those atoms having moved out of the probe beam are bounced back by the coated wall without losing their coherence and return to the probe beam again and again until they are relaxed by atom-atom or atom-wall collisions. Such alternation of optical detection and coherent spin evolution in the dark is closely related to the successive oscillatory fields method first proposed by Ramsey [41], leading to the so-called wall-induced Ramsey effect [42,43] manifested by the narrow peak on top of the transit base. The shape of the Ramsey peak in the main plot is not accurate, because the SA can only plot 400 frequency bins corresponding to a resolution of 250 Hz, which is comparable to the width of the Ramsey peak. The inset shows the undistorted Ramsey peaks from a narrower scan around the resonance center with a frequency resolution of 7.8 Hz and with transit bases subtracted. Interestingly, the Ramsey peaks for different beam

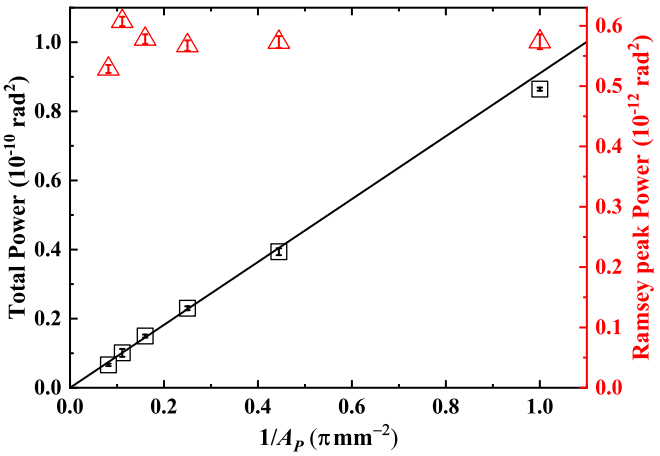

FIG. 3. The probe beam area dependence of the power of SPN. The black square represents the power of the total SPN, and the solid line is a linear fit. The red triangle represents the power of the Ramsey peak.

sizes are of equal size and can be fitted by a Lorentzian function with a full width of about 270 Hz.

By integrating the SNS, we obtain the probe beam area A_P dependence of the power of total spin noise $\delta^2\theta$ and of the Ramsey peak $\delta^2\theta_R$. As shown in Fig. 3, while $\delta^2\theta$ is inversely proportional to A_P, $\delta^2\theta_R$ is independent of A_P. Moreover, the ratio of $\delta^2\theta_R$ to $\delta^2\theta$ is equal to the ratio of A_P to the cross-section area of the vapor cell A_C for all probe beam sizes, as shown in Table I.

III. THEORETICAL ANALYSIS

A. Power of SNS

We first give a simple and intuitive explanation for our experimental results on the power of the SNS.

As shown in the inset of Fig. 1, the probe's frequency satisfies $\nu - \nu_{b,F'} \gg \nu - \nu_{a,F'} \gg \delta\nu$, where $\nu_{F,F'}$ is the optical transition frequency between the F and F' hyperfine sublevels and $\delta\nu$ represents the homogeneous linewidth of the $D1$ transition. Thus, only the polarization on the hyperfine level $a = I + 1/2$ is detected, where $I = 3/2$ is the nuclear spin of ^{87}Rb. For the simplicity of notation, we will use the symbol F_z to represent the atomic spin only on sublevel a in the following text. The probe's FR is given by [38,44]

$$\theta = \beta(\nu) n_A l \frac{\langle F_z \rangle}{2I+1}, \tag{2}$$

TABLE I. $\delta^2\theta_R/\delta^2\theta$ vs A_P/A_C for different beam sizes.

d (mm)	A_P/A_C	$\delta^2\theta_R/\delta^2\theta$
2	0.65%	0.67%
3	1.5%	1.5%
4	2.6%	2.5%
5	4.1%	3.9%
6	5.9%	6.0%
7	7.9%	7.9%

where n_A is the number density of ^{87}Rb atoms, l is the cell length, and $\langle F_z \rangle$ is averaged for atoms within the probe beam. The FR interaction cross section $\beta(\nu)$ is given by

$$\beta(\nu) \approx r_e c f \left(\frac{1}{4} \frac{1}{\nu - \nu_{a,a'}} + \frac{3}{4} \frac{1}{\nu - \nu_{a,b'}} \right), \tag{3}$$

where r_e is the classical electron radius, c is the speed of light, and f is the oscillator strength of the ^{87}Rb $D1$ transition. Then the SPN limited uncertainty of the FR is

$$\delta\theta = \frac{\partial\theta}{\partial\langle F_z \rangle} \delta F_z = \frac{\beta n_A l}{2I+1} \sqrt{\langle F_z^2 \rangle}. \tag{4}$$

For an unpolarized ensemble, the mean variance of F_z observed by the probe is given by

$$\langle F_z^2 \rangle = \frac{2a+1}{2(2I+1)} \frac{a(a+1)}{3} \frac{1}{n_A l A_P}, \tag{5}$$

where the first term is the fraction of atoms on the sublevel a, the second is the variance of F_z for a single atom, and $n_A l A_P$ is the number of atoms within the probe beam. Therefore, the noise power of FR due to SPN is

$$\delta^2\theta = \left(\frac{\beta n_A l}{2I+1} \right)^2 \langle F_z^2 \rangle = \frac{\beta^2 n_A l}{A_P} \frac{(I+1)(2I+3)}{12(2I+1)^2}. \tag{6}$$

Apply this equation to the linear fit of total noise power in Fig. 3, and we obtain the value of n_A to be 7.5×10^{12} cm^{-3}, corresponding to about 104 °C at the Rb reservoir according to Killian's formula [45]. This temperature is very close to the measured temperature at the cell's tip. At this density, the spin-exchange (SE) broadening is $q n_A \sigma_{SE} v_{rel}/\pi = 255$ Hz, where $q = 1/8$ is the nuclear slowing-down factor for the $F = 2$ hyperfine level, $\sigma_{SE} = 2 \times 10^{-14}$ cm^2 is the SE cross section, and $v_{rel} = 4.3 \times 10^4$ cm/s is the relative velocity between Rb atoms [46]. Subtracting the SE broadening from the full width of the Ramsey peak yields the wall relaxation broadening to be about 15 Hz.

The above result gives the power of total spin noise contributed by the average instantaneous fluctuation of polarization of all the atoms within the probe beam. As atoms quickly redistribute uniformly over the entire cell due to their thermal motion and coherence preserving wall collisions, the density of the atoms which have contributed to the initial polarization fluctuation and are still within the probe beam is diluted by a factor of A_P/A_C. Thus the power of the Ramsey peak can be calculated by merely changing n_A to $n_A A_P/A_C$ in Eq. (6),

$$\delta^2\theta_R = \delta^2\theta \frac{A_P}{A_C} = \frac{\beta^2 n_A l}{A_C} \frac{(I+1)(2I+3)}{12(2I+1)^2}. \tag{7}$$

Therefore, $\delta^2\theta_R$ is independent of the probe beam area and $\delta^2\theta_R/\delta^2\theta = A_P/A_C$, in complete agreement with our experimental results, as shown in Fig. 3 and Table I.

B. Line shape of the SNS

Having understood the power of spin noise, we next turn to the line shape of the SNS. In this section, we first apply the derivation of Refs. [34,38] for a flat-top probe beam to give the general expression of the diffusion autocorrelation function and the SNS. Then we compare three different theoretical models of atomic spin diffusion with the experimental SNS.

According to the Wiener-Khinchin theorem, the SNS $S(f)$ rendered by the PSD of Faraday rotation is the Fourier transform of the time autocorrelation of the FR signal $\theta(t)$:

$$S(f) = \int_0^\infty 2\langle\theta(0)\theta(\tau)\rangle \cos(2\pi f\tau)d\tau, \tag{8}$$

where the average is carried out over all the initial time zero. The FR signal θ for a flat-top probe beam is given by

$$\theta(t) = \frac{\int I(\mathbf{r})\theta_0(\mathbf{r},t)d\mathbf{r}^2}{\int I(\mathbf{r})d\mathbf{r}^2} = \frac{\int \theta_0(\mathbf{r},t)d\mathbf{r}^2}{A_\mathrm{P}}, \tag{9}$$

where the integration is over the cross section of the probe beam, $I(\mathbf{r})$ is the intensity distribution of the probe beam, and $\theta_0(\mathbf{r})$ is the mean FR for a beam of a unit area centered at $\mathbf{r}$ on the cross-sectional plane of the probe. The FR is related to the spin polarization by

$$\theta_0(\mathbf{r},t) = \beta(\nu)n_\mathrm{A}l\frac{\langle F_z(\mathbf{r},t)\rangle_0}{2I+1}, \tag{10}$$

where $\langle F_z(\mathbf{r},t)\rangle_0$ is the mean atomic spin within a beam of a unit area. Therefore, we have

$$\langle\theta(0)\theta(\tau)\rangle = \left[\frac{\beta(\nu)n_\mathrm{A}l}{(2I+1)A_\mathrm{P}}\right]^2 \times \int \langle F_z(\mathbf{r}_1,0)F_z(\mathbf{r}_2,\tau)\rangle_0 d^2\mathbf{r}_1 d^2\mathbf{r}_2. \tag{11}$$

Including the effects of the transverse magnetic field, spin diffusions, and intrinsic spin relaxation [35], the spin covariance function is given by

$$\langle F_z(\mathbf{r}_1,0)F_z(\mathbf{r}_2,\tau)\rangle_0 = \left\langle F_z^2\right\rangle_0 G(\mathbf{r}_1-\mathbf{r}_2,\tau)\cos(\omega_L\tau)e^{-\tau\Gamma_2}, \tag{12}$$

where $\Gamma_2 \equiv 1/T_2$ is the intrinsic transverse relaxation rate, $G(\mathbf{r}_1-\mathbf{r}_2,\tau)$ is the Green's function of spin diffusion, and, similar to Eq. (5),

$$\left\langle F_z^2\right\rangle_0 = \frac{2a+1}{2(2I+1)}\frac{a(a+1)}{3n_\mathrm{A}l} = \frac{(I+1)(2I+3)}{12}\frac{1}{n_\mathrm{A}l}. \tag{13}$$

Substituting Eq. (11) into (8) and using Eq. (6), we have

$$S(f) = \delta^2\theta\int_0^\infty 2C_d(\tau)\cos(\omega_L\tau)e^{-\tau\Gamma_2}\cos(2\pi f\tau)d\tau, \tag{14}$$

where ω_L is the Larmor frequency of spins under field B_y and $C_d(\tau)$ is the normalized spin diffusion autocorrelation function given by

$$C_d(\tau) = \frac{\int G(\mathbf{r}_1-\mathbf{r}_2,\tau)d^2\mathbf{r}_1 d^2\mathbf{r}_2}{A_\mathrm{P}}. \tag{15}$$

Physically, $C_d(\tau)$ represents the probability of atoms that are within the probe beam at time zero remaining inside the probe at τ, including those that leave and return to the probe beam by collisions with the cell wall or other atoms. Rigorously speaking, $C_d(\tau)$ should also take care of spin relaxations on the cell wall. However, in an evacuated ACC, wall relaxations have little effect on $C_d(\tau)$, compared to atomic diffusions, because the relaxation time due to wall collision is hundreds or even thousands of times longer than the diffusion time of an atom through the cell. Many experiments made in ACCs have confirmed that observed spin relaxations due to wall collisions approach a single-exponential decay near equilibrium, and wall relaxations can be described by an effective intrinsic relaxation rate Γ_W.

Therefore, we approximate the cell surface as a perfect reflecting boundary and treat the wall relaxation as part of the intrinsic relaxation, $\Gamma_2 = \Gamma_\mathrm{W} + \Gamma_\mathrm{SE}$, where Γ_SE represents the relaxation rate due to the spin-exchange collision, which is a real intrinsic relaxation process. Also, since the cross section of the probe beam is a circle, in order to take advantage of the cylindrical symmetry, we approximate the cross section of the vapor cell by an equivalent circle with an area equal to that of the actual square one. These approximations greatly simplify the theoretical calculation of $C_d(\tau)$.

It should be mentioned that $S(f)$ is an even function with the normalization condition given by

$$\int_{-\infty}^\infty S(f)df = \int_0^\infty 2S(f)df = \delta^2\theta. \tag{16}$$

The experimental PSD produced by the spectrum analyzer has only a positive frequency part containing the same power as its two-sided theoretical counterpart. Thus, the measured PSD is equal to $2S(f)$.

According to Eq. (14), the central task to obtain the SNS is to find the spin diffusion autocorrelation function, which depends on a correct model of spin diffusion within the ACC.

1. Fickian diffusion

Recent studies have shown that evacuated paraffin-coated Rb vapor cells contain non-negligible background gases with estimated diffusion mean free path (MFP) of Rb atoms to be about 1–2 mm or less [47,48]. Not knowing the MFP in our OTS-coated cell, we first try to use the normal diffusion, which is also called Fickian diffusion, to describe the spin transport in our system. Under this assumption, the spatial and temporal variation of the normalized spin-polarization density $\rho(r,t)$ on the cross-sectional plane of the cell is given by the Fick's diffusion equation in polar coordinates,

$$\frac{\partial\rho(r,t)}{\partial t} = D\frac{1}{r}\frac{\partial}{\partial r}\left(r\frac{\partial\rho}{\partial r}\right), \tag{17}$$

where D represents the diffusion constant. The initial and boundary conditions are, respectively, given by

$$\rho(r,0) = \begin{cases} 1/\pi R_\mathrm{P}^2, & r \leqslant R_\mathrm{P} \\ 0, & r > R_\mathrm{P} \end{cases}, \tag{18}$$

and

$$\frac{\partial\rho}{\partial r}(R_\mathrm{C},t) = 0, \tag{19}$$

where R_P is the radius of the probe beam, and $R_\mathrm{C} = 12.4\,\mathrm{mm}$ is the equivalent radius of the cell's cross section. The solution for the above equation is

$$\rho(r,t) = \frac{1}{\pi R_\mathrm{C}^2} + \sum_{n=1}^\infty k_n e^{-Dt(j_{1,n}/R_\mathrm{C})^2}J_0\left(\frac{j_{1,n}}{R_\mathrm{C}}r\right),$$
$$k_n = \frac{2}{\pi R_\mathrm{P}R_\mathrm{C}j_{1,n}J_0^2(j_{1,n})}J_1\left(\frac{j_{1,n}}{R_\mathrm{C}}R_\mathrm{P}\right), \tag{20}$$

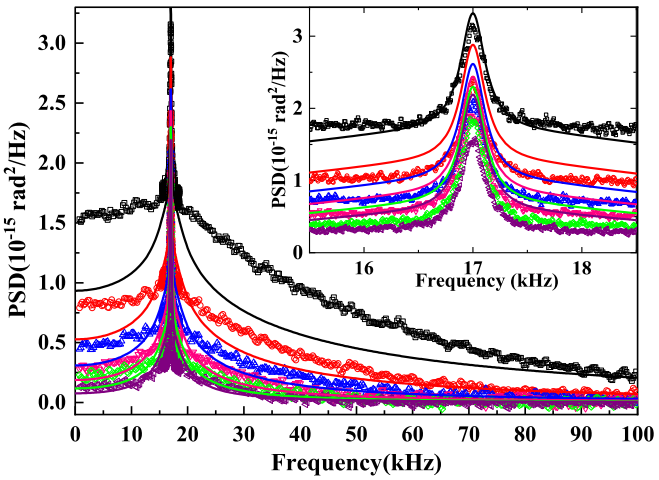

FIG. 4. The SNS fitted by the Fickian diffusion model. The inset is a zoom-in around the Ramsey peak. Empty shapes of different color represent experiment data for different probe diameters from 2 (black), 3 (red), 4 (blue), 5 (pink), and 6 (green), to 7 (purple) mm. Each solid line of the same color is the corresponding theoretical spectrum given by $2S(f)$. Each experimental curve is obtained from the spectrum of a 100-kHz scan with its data points around the resonance center being replaced by the spectrum of a 3.125-kHz scan around the resonance. The theoretical curves are generated using $D = 0.15\,\mathrm{m}^2/\mathrm{s}$.

where $J_m(x)$ is the Bessel function of the first kind of order m, and $j_{1,n}$ is the nth nonzero root of the Bessel function of order 1. The diffusion correlation function is then given by

$$C_d(\tau) = \int_0^{R_\mathrm{P}} \rho(r,\tau) 2\pi r dr,$$
$$= \frac{R_\mathrm{P}^2}{R_\mathrm{C}^2} + \sum_{n=1}^{\infty} \frac{4J_1^2\left(\frac{j_{1,n}R_\mathrm{P}}{R_\mathrm{C}}\right)}{j_{1,n}^2 J_0^2(j_{1,n})} e^{-\left(\frac{j_{1,n}}{R_\mathrm{C}}\right)^2 D\tau}, \qquad (21)$$

where the Bessel function formula, $\int xJ_0(x)dx = xJ_1(x)$, is used. Substitute the above expression of $C_d(\tau)$ into Eq. (14), and we obtain the SNS. We can see that in the final expression of $S(f)$, the first term of $C_d(\tau)$ in Eq. (21) leads to a spectrum of pure Lorentzian with a full width of Γ_2/π and an integrated area precisely equal to the power of the Ramsey peak given by Eq. (7). Therefore, the first term of $C_d(\tau)$ must represent the contribution of the Ramsey effect, and the second term the transit effect.

The numerical fitting of experimental SNS by the Fickian diffusion model is shown in Fig. 4. The first 50 $j_{1,n}$s are used to calculate $C_d(\tau)$, large enough for $C_d(0)$ to be within 5% of unity. Only one set of data corresponding to the 4-mm beam diameter ($R_\mathrm{P} = 2\,\mathrm{mm}$) is fitted using three independent fitting parameters: Γ_2, n_A, and D. The total intrinsic relaxation rate $\Gamma_2 = 270\,\pi\,\mathrm{s}^{-1}$ is obtained from the full width of the Ramsey peak. The number density n_A has already been determined from the total power of the spectrum. Therefore, only the diffusion constant D needs to be adjusted to fit the data curve. Once these three parameters are obtained, the theoretical spectra for other beam sizes are automatically generated based on their values of R_P. As shown in Fig. 4, Fickian diffusion fails to describe the spin motion in the ACC.

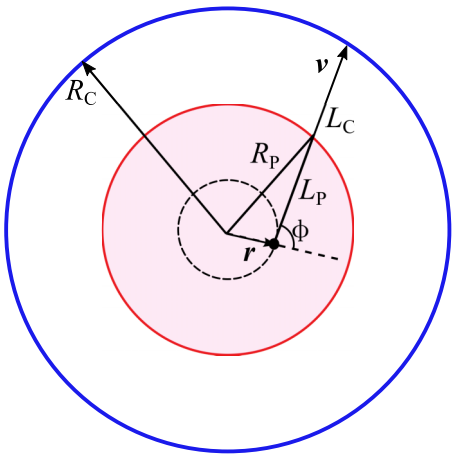

FIG. 5. Schematics of an atom's flying path in the cell. R_C: radius of the cell; R_P: radius of the probe beam; **r**: initial position of an atom; **v**: atom's initial velocity; ϕ: the relative angle between **v** and **r**; L_P: distance the atom travels to exit the probe; L_C: distance the atom travels to reach the cell wall.

2. *Ballistic flight*

In this section, we assume that atoms take ballistic flight in the cell between successive wall collisions. A similar model has been used to study the absorption profile of electromagnetically induced transparency in paraffin-coated cells [49]. Here, the velocity of the atom obeys Maxwell distribution, which, in two-dimensional cases, is given by

$$f_2(v) = \frac{1}{2\pi\langle v_x^2\rangle} \exp\left(-\frac{v^2}{2\langle v_x^2\rangle}\right),$$
$$\langle v_x^2\rangle = k_B T/m, \qquad (22)$$

where $\langle v_x^2\rangle$ is the atom's one-dimensional mean square velocity, k_B is the Boltzmann constant, m is the mass of an ^{87}Rb atom and T is the temperature of the vapor, which is equal to the cell's body temperature.

As shown in Fig. 5, suppose an atom's initial position is at **r** from the center of the probe and initial velocity is given by (v, ϕ) in the polar coordinate shown in the figure; the distance it needs to travel to exit the probe beam is given by

$$L_\mathrm{P}(r,\phi) = \sqrt{R_\mathrm{P}^2 - r^2\sin^2\phi} - r\cos(\phi). \qquad (23)$$

Averaging the atoms' velocity distribution and initial positions, we obtained the probability for atoms initially within the probe beam to keep staying inside the beam at τ:

$$P_\mathrm{S}(\tau) = \int_0^{R_\mathrm{P}} \frac{2\pi r dr}{\pi R_\mathrm{P}^2} \int_0^{2\pi} d\phi \int_0^{L_\mathrm{P}(r,\phi)/\tau} v f_2(v) dv. \qquad (24)$$

Besides the atoms that never leave the probe beam, we also need to count the atoms that exit and then return to the probe by colliding with the cell wall. Since an atom's velocity is thermalized after bouncing off the coated cell wall [50], to a first rough approximation, we assume that once an atom hits the wall, it is suddenly redistributed uniformly inside the cell. Then its probability of residing within the probe beam is equal

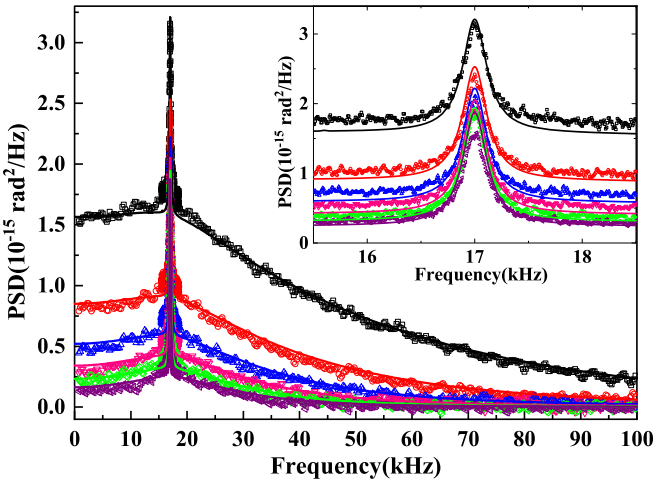

FIG. 6. The SNS fitted by the ballistic flight model. The inset shows a zoom-in around the Ramsey peak. The color coding is the same as that of Fig. 4.

to the ratio between the cross-sectional areas of the beam and the cell, A_P/A_C. Therefore, $C_d(\tau)$ can be written as

$$C_d(\tau) \approx P_S(\tau) + P_B(\tau)\frac{A_P}{A_C}, \tag{25}$$

where $P_B(\tau)$ is the probability for atoms initially within the probe beam of having hit the cell wall by time τ:

$$P_B(\tau) = \int_0^{R_P} \frac{2\pi r dr}{\pi R_P^2} \int_0^{2\pi} d\phi \int_{L_C(r,\phi)/\tau}^{\infty} v f_2(v) dv, \tag{26}$$

where $L_C(r,\phi)$ represents the distance the atom needs to travel to hit the cell wall:

$$L_C(r,\phi) = \sqrt{R_C^2 - r^2\sin^2\phi} - r\cos(\phi). \tag{27}$$

Substituting $C_d(t)$ into Eq. (14), we obtain the final SNS.

Note, we have assumed a sudden redistribution of atoms upon their arrival at the cell wall. However, an atom needs to travel more distance to return to the probe. A better approximation would be to construct a fictitious circle of radius R_f larger than R_C, and to allow atoms to fly through the cell wall and be suddenly redistributed upon hitting this fictitious boundary. By choosing R_C as the boundary of sudden redistribution in Eq. (27), we effectively increase the value of $P_B(\tau)$ and cause $C_d(\tau)$ to decay more slowly, according to Eq.(25).

The fitting procedure is similar to the Fickian diffusion model, except that there are now only two independent parameters: Γ_2 and n_A, which have the same value as before. As shown in Fig. 6, the fitting looks much better than that of Fickian diffusion. However, we can still see that the transit base of the theoretical curve is slightly broader than the experimental one, especially on the left shoulder. Since a broader spectrum corresponds to a faster decay, this means that the theoretical $C_d(\tau)$ decays more quickly than the experimental one. To improve the fitting, we need to change R_C in Eq. (27) to a smaller radius to let Rb atoms return to the probe before they reach the cell wall. This inconsistency of the ballistic flight model indicates the existence of non-negligible background gases, yet the superiority of the ballistic flight model over the Fickian diffusion also suggests that the atomic MFP is probably larger than the diameter of the probe beam so that the probe sees more straight flights than zigzag diffusions of the atoms.

3. *Langevin's diffusion*

According to the theory of Brownian motion, if the distance scale of interest such as the probe beam's diameter is comparable or smaller than the mean free path, then the atomic motion should be better described by Langevin's theory of diffusion, which we will examine in this section.

The Green's function for an unrestricted one-dimensional Langevin's diffusion starting from the origin is given by [51]

$$G(x,t) = \frac{1}{\sqrt{2\pi\langle x^2(t)\rangle}} \exp\left[-\frac{x^2}{2\langle x^2(t)\rangle}\right], \tag{28}$$

where $\langle x^2(t)\rangle = 2D[t - \tau_D(1 - e^{-t/\tau_D})]$ and $\tau_D = Dm/k_BT$. Relating the partial derivatives of $G(x,t)$ with respect to t and x yields the following equation:

$$\frac{\partial G(x,t)}{\partial t} = D(1 - e^{-t/\tau_D})\frac{\partial^2 G}{\partial x^2}. \tag{29}$$

Regarding this as the one-dimensional Langevin's diffusion equation, we can then change $G(x,t)$ to $\rho(x,t)$, and generalize the equation to its two-dimensional polar form,

$$\frac{\partial \rho(r,t)}{\partial t} = D(1 - e^{-t/\tau_D})\frac{1}{r}\frac{\partial}{\partial r}\left(r\frac{\partial \rho}{\partial r}\right), \tag{30}$$

with the same initial and boundary conditions as Eqs. (18) and (19), respectively. The solution of Eq. (30) is

$$\rho(r,t) = \frac{1}{\pi R_C^2} + \sum_{n=1}^{\infty} k_n e^{-D(t+\tau_D e^{-t/\tau_D})\left(\frac{j_{1,n}}{R_C}\right)^2} J_0\left(\frac{j_{1,n}}{R_C}r\right),$$

$$k_n = \frac{2e^{D\tau_D\left(j_{1,n}/R_C\right)^2}}{\pi R_P R_C j_{1,n} J_0^2(j_{1,n})} J_1\left(\frac{j_{1,n}}{R_C}R_P\right). \tag{31}$$

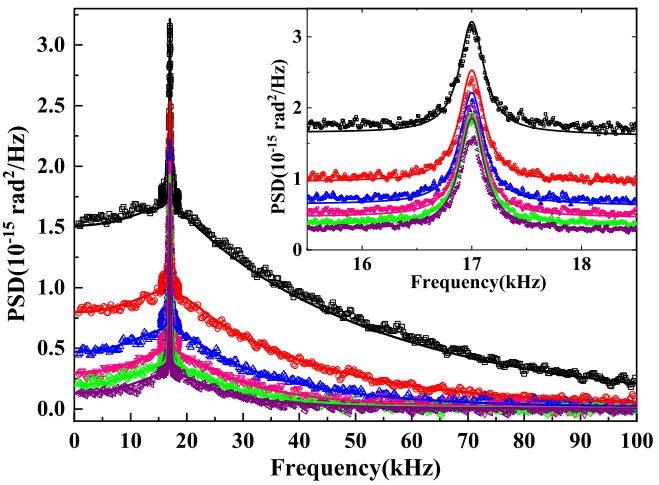

FIG. 7. The SNS fitted by Langevin's diffusion model. The inset shows a zoom-in at the Ramsey peak. The color coding is the same as that of Fig. 4.

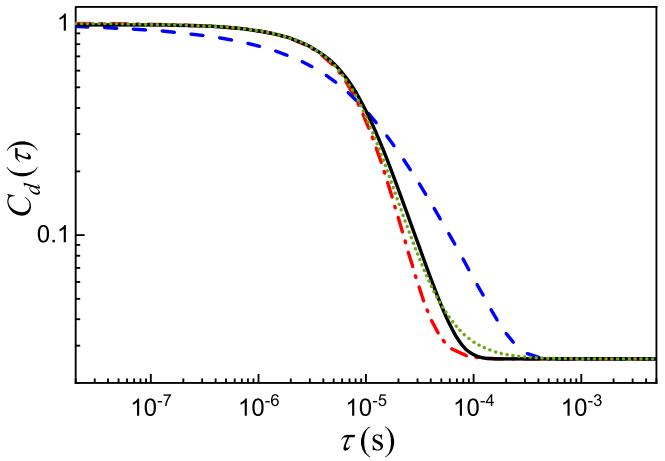

FIG. 8. Calculated diffusion correlation functions of different models for the 2-mm beam radius. They belong to Fickian diffusion (blue dash), ballistic flight with $R_f = R_C$ (red dash-dot) and $R_f =$ 2 mm (green dot), and Langevin's diffusion (black solid).

We notice that the solution of Langevin's diffusion can be obtained from that of the Fickian diffusion by replacing Dt in the latter with $D[t - \tau_D(1 - e^{-t/\tau_D})]$. Similar to Eq. (21), the diffusion correlation function is found to be

$$C_d(\tau) = \frac{R_P^2}{R_C^2} + \sum_{n=1}^{\infty} \frac{4J_1^2\left(j_{1,n}\frac{R_P}{R_C}\right)}{j_{1,n}^2 J_0^2(j_{1,n})} e^{-\left(\frac{j_{1,n}}{R_C}\right)^2 D[\tau - \tau_D(1-e^{-\tau/\tau_D})]}. \quad (32)$$

The fitting of the experimental SNS using the Langevin's diffusion model is shown in Fig. 7. The fitting procedure is the same as that of the Fickian diffusion, and the first two independent parameters, Γ_2 and n_A, remain the same as before. The best fit yields $D = 0.6\,\mathrm{m}^2/\mathrm{s}$, corresponding to a mean free path $\lambda = 6$ mm by the relation $\lambda = 3D/\bar{v}$, where $\bar{v}$ is the mean thermal speed. As shown in Fig. 7, the simultaneous match between the theoretical and the experimental SNS for different beam sizes with a single value of D is remarkable. The content of the background gas in OTS-coated cells has been found to be mostly light hydrocarbon molecules [52]. If the cross section of velocity changing collision $\sigma_C \sim 1 \times 10^{-14}\,\mathrm{cm}^2$, the pressure of the background gas is given by $p = k_B T/\lambda\sigma_C \sim 0.8$ Pa [47].

In Fig. 8, we compare the calculated diffusion correlation functions of all three models for the case of $R_P = 2$ mm. It is interesting to see that by reducing the radius of the fictitious boundary for the ballistic flight model, we can change its $C_d(\tau)$ to be very close to that of Langevin's diffusion.

As a last note, we can easily verify that in all three models, if $R_P \to R_C$, then $C_d(\tau) \to 1$. The SNS will then reduce to a single Lorentzian Ramsey peak with no transit base. Because the previous vapor cell is bigger than the optical window of the cell oven, we have made another OTS-coated cell with a cross section of 8 mm × 8 mm, allowing the probe beam to cover the entire cell, and the above prediction is confirmed.

IV. CONCLUSIONS

In summary, we experimentally studied the spin-noise spectrum (SNS) of hot ^{87}Rb vapor atoms inside an anti-relaxation OTS-coated cell with flat-top probe beams of different diameters. We found that SNS consists of two distinct parts, which are a broad transit base and a narrow Ramsey peak. The power of the total spin noise is inversely proportional to the probe beam area while the power, as well as the line shape of the Ramsey peak, is independent of the probe beam size. The ratio between the two powers is equal to the ratio between the cross-sectional areas of the vapor cell and the probe beam. A simple theoretical explanation is given. Combining with the fact that the field response of a magnetometer is independent of the probe beam size, we conclude that the fundamental sensitivity limit of a magnetometer in an anti-relaxation-coated cell depends on the probe beam area.

To give a full account of the line shape of the SNS, we examined three theoretical models of diffusion: Fickian diffusion, ballistic flight, and Langevin's diffusion. Fickian diffusion fails to fit the line shape. The ballistic flight model gives satisfactory fitting results and can be further improved by assuming atoms bouncing off from a fictitious boundary inside the cell, which is not consistent with its original assumption. Langevin's diffusion yields the best agreement with the experiment while being self-consistent. A mean free path (MFP) of 6 mm is found in our cell by this model. The fact that this MFP is larger than or comparable to the probe beam size but smaller than the cell size is precisely the reason Langevin's diffusion is required. If the MFP is much larger than the cell diameter, then the ballistic flight model will be excellent. If it is much smaller than the probe beam size, such as in ACCs filled with a small amount (several Torrs) of N_2 quenching gas, then the normal Fickian diffusion model will be valid.

Despite giving different spectrum line shapes, all three diffusion models yield the same result for the power of the spin noise. This is because they adopt the same approximation, where we regard the cell wall as a perfect reflecting boundary and treat the wall relaxation as part of the intrinsic relaxation instead of entailing it in the boundary condition. Such approximation is valid for high-quality coated cells where the relaxation probability for a single wall collision is much smaller than the ratio of MFP to the average cell diameter [53]. We also notice that the independence of the total spin noise power on the detailed mechanisms of spin diffusion and relaxation as indicated by Eq. (6) suggests a simple method for determining the number density of thick atomic vapors.

ACKNOWLEDGMENTS

We thank Professor Y. H. Xiao for lending us the π shaper and Professor X. J. Ning for helpful discussions. This work is supported by the National Key Research Program of China under Grant No. 2016YFA0302000, NNSFC under Grant No. 91636102 and the Natural Science Foundation of Shanghai under Grant No. 16ZR1402700.

[1] D. Budker and M. Romalis, Nat. Phys. **3**, 227 (2007).

[2] I. K. Kominis, T. W. Kornack, J. C. Allred, and M. V. Romalis, Nature **422**, 596 (2003).

[3] *Optical Magnetometry*, edited by D. Budker and D. F. J. Kimball (Cambridge University Press, Cambridge, 2013).

[4] T. G. Walker and M. S. Larsen, in *Advances in Atomic, Molecular, and Optical Physics, Vol. 65*, edited by E. Arimondo, C. C. Lin, and S. F. Yelin (Elsevier Academic Press Inc., San Diego, 2016), pp. 373–401.

[5] T. W. Kornack, R. K. Ghosh, and M. V. Romalis, Phys. Rev. Lett. **95**, 230801 (2005).

[6] T. E. Chupp, P. Fierlinger, M. J. Ramsey-Musolf, and J. T. Singh, Rev. Mod. Phys. **91**, 015001 (2019).

[7] J. M. Brown, S. J. Smullin, T. W. Kornack, and M. V. Romalis, Phys. Rev. Lett. **105**, 151604 (2010).

[8] J. Lee, A. Almasi, and M. Romalis, Phys. Rev. Lett. **120**, 161801 (2018).

[9] M. S. Safronova, D. Budker, D. DeMille, D. F. J. Kimball, A. Derevianko, and C. W. Clark, Rev. Mod. Phys. **90**, 025008 (2018).

[10] M. P. Ledbetter, I. M. Savukov, V. M. Acosta, D. Budker, and M. V. Romalis, Phys. Rev. A **77**, 033408 (2008).

[11] H. G. Robinson, E. S. Ensberg, and H. G. Dehmelt, Bull. Am. Phys. Soc. **3**, 9 (1958).

[12] M. A. Bouchiat and J. Brossel, Phys. Rev. **147**, 41 (1966).

[13] M. V. Balabas, K. Jensen, W. Wasilewski, H. Krauter, L. S. Madsen, J. H. Müller, T. Fernholz, and E. S. Polzik, Opt. Express **18**, 5825 (2010).

[14] M. V. Balabas, T. Karaulanov, M. P. Ledbetter, and D. Budker, Phys. Rev. Lett. **105**, 070801 (2010).

[15] S. J. Seltzer and M. V. Romalis, J. Appl. Phys. **106**, 114905 (2009).

[16] K. F. Zhao and Z. Wu, Appl. Phys. Lett. **89**, 261113 (2006).

[17] G. Vasilakis, H. Shen, K. Jensen, M. Balabas, D. Salart, B. Chen, and E. S. Polzik, Nat. Phys. **11**, 389 (2015).

[18] D. Budker, D. F. Kimball, S. M. Rochester, V. V. Yashchuk, and M. Zolotorev, Phys. Rev. A **62**, 043403 (2000).

[19] J. Vanier, J. F. Simard, and J. S. Boulanger, Phys. Rev. A **9**, 1031 (1974).

[20] D. Budker, L. Hollberg, D. F. Kimball, J. Kitching, S. Pustelny, and V. V. Yashchuk, Phys. Rev. A **71**, 012903 (2005).

[21] B. Julsgaard, A. Kozhekin, and E. S. Polzik, Nature **413**, 400 (2001).

[22] C. Schori, B. Julsgaard, J. L. Sorensen, and E. S. Polzik, Phys. Rev. Lett. **89**, 057903 (2002).

[23] W. Li, M. Balabas, X. Peng, S. Pustelny, A. Wickenbrock, H. Guo, and D. Budker, J. Appl. Phys. **121**, 063104 (2017).

[24] S. A. Crooker, D. G. Rickel, A. V. Balatsky, and D. L. Smith, Nature **431**, 49 (2004).

[25] E. B. Aleksandrov and V. S. Zapassky, Zh. Eksp. Teor. Fiz. **81**, 132 (1981).

[26] V. S. Zapasskii, Adv. Opt. Photonics **5**, 131 (2013).

[27] N. A. Sinitsyn and Y. V. Pershin, Rep. Prog. Phys. **79**, 106501 (2016).

[28] V. S. Zapasskii, A. Greilich, S. A. Crooker, Y. Li, G. G. Kozlov, D. R. Yakovlev, D. Reuter, A. D. Wieck, and M. Bayer, Phys. Rev. Lett. **110**, 176601 (2013).

[29] P. Glasenapp, N. A. Sinitsyn, L. Y. Yang, D. G. Rickel, D. Roy, A. Greilich, M. Bayer, and S. A. Crooker, Phys. Rev. Lett. **113**, 156601 (2014).

[30] V. G. Lucivero, R. Jimenez-Martinez, J. Kong, and M. W. Mitchell, Phys. Rev. A **93**, 053802 (2016).

[31] M. Oestreich, M. Romer, R. J. Haug, and D. Hagele, Phys. Rev. Lett. **95**, 216603 (2005).

[32] S. A. Crooker, J. Brandt, C. Sandfort, A. Greilich, D. R. Yakovlev, D. Reuter, A. D. Wieck, and M. Bayer, Phys. Rev. Lett. **104**, 036601 (2010).

[33] J. Hubner, F. Berski, R. Dahbashi, and M. Oestreich, Phys. Status Solidi B **251**, 1824 (2014).

[34] G. M. Muller, M. Romer, D. Schuh, W. Wegscheider, J. Hubner, and M. Oestreich, Phys. Rev. Lett. **101**, 206601 (2008).

[35] Y. V. Pershin, V. A. Slipko, D. Roy, and N. A. Sinitsyn, Appl. Phys. Lett. **102**, 202405 (2013).

[36] A. V. Poshakinskiy and S. A. Tarasenko, Phys. Rev. B **92**, 045308 (2015).

[37] D. Sheng, S. Li, N. Dural, and M. V. Romalis, Phys. Rev. Lett. **110**, 160802 (2013).

[38] V. G. Lucivero, N. D. McDonough, N. Dural, and M. V. Romalis, Phys. Rev. A **96**, 062702 (2017).

[39] G. Zhang, L. Wei, M. Wang, and K. Zhao, J. Appl. Phys. **117**, 043106 (2015).

[40] A. L. Marchant, S. Händel, T. P. Wiles, S. A. Hopkins, C. S. Adams, and S. L. Cornish, Opt. Lett. **36**, 64 (2011).

[41] N. F. Ramsey, Rev. Sci. Instrum. **28**, 57 (1957).

[42] H. M. Goldenberg, D. Kleppner, and N. F. Ramsey, Phys. Rev. **123**, 530 (1961).

[43] S. I. Kanorsky, A. Weis, and J. Skalla, Appl. Phys. B-Lasers Opt. **60**, S165 (1995).

[44] W. Happer and B. S. Mathur, Phys. Rev. **163**, 12 (1967).

[45] T. Killian, Phys. Rev. **27**, 578 (1926).

[46] W. Happer and H. Tang, Phys. Rev. Lett. **31**, 273 (1973).

[47] N. Sekiguchi and A. Hatakeyama, Appl. Phys. B **122**, 81 (2016).

[48] A. Hatakeyama, T. Kuroda, N. Sekiguchi, and K. Ishikawa, Appl. Phys. B **125**, 133 (2019).

[49] M. Klein, M. Hohensee, D. F. Phillips, and R. L. Walsworth, Phys. Rev. A **83**, 013826 (2011).

[50] N. Sekiguchi, A. Hatakeyama, K. Okuma, and H. Usui, Phys. Rev. A **98**, 042709 (2018).

[51] D. T. Gillespie and E. Seitaridou, *Simple Brownian Diffusion: An Introduction to the Standard Theoretical Models*, 1st ed. (Oxford University Press, Oxford, UK, 2012).

[52] Y. W. Yi, H. G. Robinson, S. Knappe, J. E. Maclennan, C. D. Jones, C. Zhu, N. A. Clark, and J. Kitching, J. Appl. Phys. **104**, 023534 (2008).

[53] W. Happer and W. A. Vanwijngaarden, Hyperfine Interact. **38**, 435 (1987).